SSRG International Journal of Electronics and Communication Engineering
ISSN: 2348-8549/ https://doi.org/10.14445/23488549/IJECE-V12I4P109

Volume 12 Issue 4, 99-109, April 2025

Original Article

Four-Element Four-Port Mushroom-Shaped MIMO Antenna System with Enhanced Diversity and Desirable Radiation for Sub-6 GHZ 5G Smartphones

Anuradha P. Kulkarni[1]*, Jayashree P. Shinde[2], Pratap N. Shinde[3]

[1,2]*Department of Electronics and Communication, Sinhgad Academy of Engineering, Sinhgad Kondwa, Danny Mehata Nagar, Kondhwa, Pune, Yewalewadi, Maharashtra, India.*
[3]*Department of Electronics and Communication, TSSM's Bhivarbai Sawant College of Engineering, Gate Number 1, Near BSCOER, Narhe, Pune, Maharashtra, India.*

**Corresponding Author : anuradhak.kulkarni@gmail.com*

Received: 06 February 2025 Revised: 08 March 2025 Accepted: 09 April 2025 Published: 29 April 2025

Abstract *- With the rapid advancement of 5G networks, the demand for efficient, compact, and multi-functional smartphone antennas has increased significantly. This paper presents the design and analysis of a compact Four-Element, Four-Port mushroom-shaped MIMO antenna system optimized for sub-6 GHz 5G smartphone applications to address these requirements. The proposed antenna array utilizes mushroom structures and Defected Ground Structures (DGS) to enhance polarization diversity, improve isolation, and suppress mutual coupling without complex decoupling networks. Designed on an FR-4 substrate with miniaturized radiators, the antenna system is optimized for space-constrained smartphone platforms, offering full radiation coverage and multiple resonance points. Simulated results demonstrate efficient radiation patterns, low reflection coefficients (below -10 dB), and excellent MIMO performance, with low Envelope Correlation Coefficients (ECC) below 0.04 through the entire frequency band. The design is well-suited for future 5G devices, ensuring reliable performance and high spectral efficiency for multi-band, multi-port communication systems.*

Keywords *- Defected Ground Structure, MIMO, Mushroom shape, Patch antenna, Smartphone, sub-6 GHz.*

1. Introduction

The emergence of 5G mobile networks addresses the limitations of current 4G systems in supporting high-data transfer rates and accommodating future wireless communication demands [1]. Massive MIMO, mobile broadband, Machine-To-Machine (M2M), Internet of Things (IoT), and ultra-reliable connections are among the key services that 5G seeks to enhance. Implementing advanced multi-element antenna designs is crucial for realizing the full potential of 5G, particularly in improving network reliability and optimizing spectral efficiency [2-4]. MIMO technology, which employs multiple resonators, significantly enhances wireless channel capacity without requiring additional power, making it a fundamental aspect of next-generation networks [5]. Already utilized in 4G LTE, MIMO is set to play a pivotal role in 5G networks by transmitting signals through uncorrelated antennas to mitigate fading and improve link consistency [6, 7]. For 5G mobile terminals, especially handheld devices, achieving high efficiency with compact, low-profile antennas that offer sufficient bandwidth and minimal Mutual Coupling (MC) is essential. However, the restricted space on smartphone mainboards presents significant challenges for integrating large-scale antenna arrays. Microstrip (Ms) antennas, known for their affordability and ease of integration, offer a promising solution for cellular operations. Their planar structure and straightforward design make them ideal for smartphone applications, ensuring efficient performance while maintaining a small footprint [8].

The Federal Communications Commission (FCC) has designated the millimetre-wave (mm-wave) spectrum, including frequencies like 24 GHz, 28 GHz, 37–39 GHz, and 60 GHz, for 5G communication. However, mm-wave frequencies suffer from severe propagation losses, making them unsuitable for consistent mobile applications. To address this issue, the International Telecommunication Union (ITU) has emphasized using the sub-6 GHz mid-band, which provides broader coverage with reduced propagation challenges. MIMO technology has played a crucial role in enhancing spectral efficiency and link robustness, particularly in rich multipath environments, where it significantly increases system capacity. As a result, MIMO remains essential for meeting the demands of modern wireless networks, including 4G, 5G, and future 6G applications,

enabling the development of compact, highly integrated, and autonomous communication systems across various sectors [9]. Despite the advancements in MIMO technology, a significant research gap remains in addressing the challenge of minimizing MC and Envelope Correlation Coefficient (ECC) among closely spaced antennas. Conventional approaches to mitigating MC involve employing Decoupling Networks (DN), which, although practical, add complexity to the antenna design. Alternative isolation techniques, such as introducing slots, rectangular defective ground structures, and slitted patterns in the Ground Plane (GP), can enhance isolation but often degrade the antenna's radiation pattern. As the number of antennas in a compact mobile terminal increases, these challenges become more pronounced, negatively impacting Antenna System (AS) efficiency [10, 11].

Recent smartphone antenna designs for 5G applications, particularly those operating below 6 GHz, have predominantly relied on single-polarized resonators with non-planar configurations, resulting in limited Radiation Coverage (RC) and excessive mainboard space consumption. To overcome these limitations, this work presents a novel four-element MIMO antenna system featuring miniature polarization-diverse mushroom-shaped resonators.

The proposed design achieves full radiation coverage while maintaining a compact structure and high isolation without requiring additional DNs. Each resonator is fed by independent T-shaped feed lines, ensuring optimal performance. The proposed antenna array is designed and optimized using the commercially available HFSS software package, demonstrating significant miniaturization and improved isolation characteristics compared to existing designs.

The contribution of this article is as follows:

- To fit within smartphone constraints, a compact 5G MIMO antenna array using mushroom resonators is designed for efficient integration.
- To improve radiation patterns, mushroom structures fine-tune current distribution, achieving diverse characteristics in a smaller size.
- To minimize mutual coupling, DGS enhance polarization diversity and suppresses unwanted coupling.
- Semi-circular slots manipulate current flow to boost bandwidth and isolation, eliminating complex isolation circuits and reducing interference.

The paper is arranged as follows: Chapter 2 explains the existing works with their benefits and limitations in detail, Chapter 3 describes the strategy of the antenna element, Chapter 4 provides the simulated outcome and its discussion, and Chapter 5 concludes the paper with references provides the future research direction and Chapter 6 concludes the paper with references.

2. Literature Review

Ghadeer et al. [12] developed a compact AS comprising four radiating elements for 5G MIMO applications. These elements featured mushroom curves and were excited using an open-circuited feed line via CPW. A ground organization with low-high-low impedance among radiating elements was incorporated to broaden the array's impedance bandwidth. This structure, characterized by a staircase configuration inclined along the input feedline, effectively minimized R among adjacent radiators. A CRLH-based band reject filter, utilizing Hilbert mushroom geometry, was integrated at the array's rear to mitigate MC. The antenna, which covered frequencies ranging from 2 to 3 GHz, 3.4–3.9 GHz, and 4.4–5.2 GHz, was fabricated and tested, demonstrating its suitability for 5G communication systems. However, the band reject filter based on the CRLH structure faced challenges due to manufacturing inconsistencies and environmental factors, potentially impacting its filtering performance over time.

Jaglan et al. [13] presented an 18-element antenna system compatible with massive MIMO/diversity 4G/5G SP, operating within sub-6 GHz LTE bands 42 (3.4-3.6 GHz) and 43 (3.6-3.8 GHz). They employed a simple slot-type antenna design with open-ended slots for compactness, and the antennas also functioned as decoupling elements to enhance isolation between radiators. Using a low-cost FR-4 substrate measuring 150 mm × 80 mm × 1.6 mm, suitable for a 6-inch SP, the proposed elements demonstrated simulated and measured gains exceeding 5.3 dBi. Throughout the operating Frequency Range (FR), the design exhibited exceptional impedance equivalent (reflection factor >20 dB), port isolation (I) (>20 dB), overall efficacy (>87%), and ECC (<0.01). However, despite employing open-ended slots, achieving high isolation in a densely packed 18-element array remained challenging due to MC among closely spaced AS.

Cholavendan et al. [14] designed a compact dual-feed MIMO AS for a sub-6 GHz 5G model, focusing on isolation enhancement-each patch of the proposed antenna utilized two orthogonal inset-feed lines to resonate at 3.65 GHz. Diagonal stubs, implemented via plated through-hole technology between orthogonal ports, ensured minimal inter-port isolation (≤ −12 dB) for each patch. This structure, forming an 8-element miniaturized MIMO antenna, was validated through fabricated prototypes that confirmed the simulation results. A decoupling structure integrated into the GP facilitated the achievement of various performance factors, including envelope correlation (≤ −15 dB). ECC, Diversity Gain (DG), and MEG measurements fell within acceptable ranges. However, the fixed resonance at 3.65 GHz may have hindered adaptability to diverse sub-6 GHz bands in SP, potentially restricting bandwidth coverage. Hadri et al. [15] designed a small, quad-element MIMO antenna for satellites and 5G communication networks. A CPW line supplied power to each antenna's four identical elements perpendicularly on a 40 × 40 mm² FR-4 substrate. Effective matching was achieved

across the lower (4.9 GHz) and upper (17 GHz) frequency ranges by incorporating two slits and an I-shaped slot into the patch and modifying its parameters. Additionally, stubs placed on the ground plane and polarization diversity techniques produced 25 dB and 30 dB isolations in the lower and upper bands, respectively. Measurements were conducted on a fabricated antenna prototype to validate its performance in terms of Diversity Gain (DG), efficiency, Reflection Coefficient (RC), Envelope Correlation Coefficient (ECC), and Total Active Reflection Coefficient (TARC). The effectiveness of the proposed MIMO AS was confirmed by the measured results, which showed good agreement with the expected performance. However, its narrow frequency band (4.9 GHz and 17 GHz) limited its adaptability for wider frequency ranges, likely requiring modifications for broader applications.

Kiani et al. [16] revealed an eight-element slotted Wideband (Wb) MIMO AS designed to operate in the N77 (3.2–4.2 GHz) frequency range. The antennas were carefully positioned along the size and width of the PCB to provide design and polarization diversity, enhancing signal reception from multiple directions. The PCB was printed on a 150 × 75 mm² FR-4 substrate with a thickness of 0.8 mm. Wideband characteristics in the 3.25–4.49 GHz range were achieved using a T-slot and an inverted C-slotted stub. All MIMO components exhibited radiation and overall efficiency above 60%. A slot was added to improve isolation among antenna elements along the PCB's width, resulting in 14.5 dB isolation. This helped achieve an extreme channel capacity of 40 bps/Hz, Diversity Gain (DG) >9.95 dB, and Envelope Correlation Coefficient (ECC) <0.025. However, the isolation of 14.5 dB among PCB-placed antennas may not have met high-performance MIMO requirements aiming for >20 dB isolation, necessitating further isolation techniques.

Parchin et al. [17] presented a MIMO AS with broad radiation and Diversity Gain (DG) designed for sub-6 GHz 5G cellular models. Four sets of miniature square-loop resonators with independent T-shaped feed lines and dual polarization were strategically positioned at the edge curves of a smartphone that measured 75 mm by 150 mm. Each pair operated in the 3.6 GHz frequency spectrum and featured resonators that were polarised both horizontally and vertically. A square slot was positioned and activated beneath each loop resonator to achieve the desired isolation between neighbouring elements without additional decoupling systems, enhancing frequency bandwidth and radiation coverage.

Al-Ani et al. [18] presented a dual-polarization four-antenna MIMO scheme, with the elements arranged on a 67 × 139 mm² PCB using an FR-4 dielectric substrate (εr = 4.4, thermal conductivity = 0.025). A circular slot radiator was integrated into the ground plane to enhance radiation properties. Two rectangular parasitics with one open rib were inserted through the square slot radiator to reduce mutual coupling. The single antenna system extended to 1.47 MHz (5.48–6.95 GHz) at -6 dB, covering a frequency range of 5.81–6.66 GHz at -10 dB impedance matching. The results demonstrated -20 dB return losses and -45 dB isolation. For future 5G wireless communications, the proposed antenna system could be integrated into new smartphone devices. Kulkarni et al. [19] presented a miniature stacked patch antenna designed for Internet of Things applications, utilizing dual linear polarization in the WiMAX frequency band and circular polarization in the GPS L1 channel. Integrating pi-shaped slots and an additional reflective patch with shorting pins was a novel approach to enhancing a dual-band patch antenna. The upper patch functioned as a separate receiver in the WiMAX band by employing an improved design for the base patch.

Fakharian et al. [20] unveiled a switchable array of antennas designed for future massive MIMO smartphone applications in 4G and 5G. The antenna consisted of two modules: a 6×6 MIMO 5G antenna system with pattern diversity and a switchable 2×2 MIMO 4G antenna system with frequency and rounded polarization ranges. Each module component, including a spiral patch and a short-ended C-shaped stub as a parasitic feature, was fed through a microstrip line with a tuned slot on the ground plane. Each element occupied an area of 22 × 9.3 mm² on the ground plane. Spatial diversity and polarization methods were employed to enhance isolation and reduce coupling effects. To meet the requirements of future 5G models, the 5G antenna system operated in the 3.4–3.6 GHz range, while the 4G antenna system could switch between the LTE-2500 and 5G bands by integrating a PIN diode into the antenna structure.

Sghaier et al. [21] developed a wideband MIMO antenna system for 5G new radio models in future smartphones, operating in the frequency band from 3.3 to 7.1 GHz. An FR-4 printed circuit board was used for the antenna system, with four small microstrip-fed slot antennas positioned at its junctions. Two L-shaped microstrip feeding cables supplied power to a radiator that contained two concentric annular slots in each antenna system. The feed lines were arranged orthogonally to provide polarization diversity and a variety of emission patterns. The two rings were joined and connected by a small gap to link and shift the resonant modes for radiation control, while rectangular slots were placed beneath each microstrip feed line to reduce mutual coupling.

Alaa et al. [22] suggested three MIMO antenna systems with various configurations to achieve polarization and spatial diversities for upcoming wireless communication applications in the Q-band frequency. The MIMO antenna systems were built using a single element, a Circularly Polarised (CP) printed antenna system that operated at 37.8 and 50 GHz. A four-element MIMO antenna system was created to achieve polarization and spatial diversity. In contrast, two-element

MIMO antenna systems placed side-by-side and face-to-face were proposed to achieve diversity gain. The CST simulator was used to evaluate the proposed MIMO antenna systems. The fabricated antenna system's circular polarization, impedance matching, axial gain, envelope correlation coefficient, and diversity gain were assessed empirically. The strong alignment between simulation and test results for the single-element and MIMO antenna systems demonstrated high performance.

Chaudhary et al. [23] developed a planar low-profile wideband Circularly Polarised (CP) MIMO antenna system that provided pattern and polarization variation throughout the Axial-Ratio Bandwidth (ARBW) and operated in the X-band. The design incorporated a ground plane between two polarised monopole antenna systems to achieve wideband CP, pattern diversity, and high isolation among antenna systems. With isolation better than 20 dB, the MIMO antenna system demonstrated an impedance balancing bandwidth of 3.52 GHz (8.07–11.59 GHz) and an ARBW of 2.45 GHz (8.11–10.56 GHz) with 3 dB. It was emphasized that the antenna system could be easily scaled to operate in various frequency bands. Its performance was evaluated against several antenna systems and was fabricated on an FR-4 substrate.

3. Design of The Four-Element Four-Port Mushroom-Shaped Mimo Antenna

The suggested Four-Element Four-Port Mushroom-shaped MIMO AS is depicted in Figure 1(a). Ant 1 through Ant 4 are the numbers of its four AS. The FR-4 material on which these AS are constructed has a loss tangent of 0.02 and an average permit amount of 4.4. Placing the antennas at the corners allows for better exploitation of the space available in SP form factors while providing optimized radiation patterns in multiple directions. With dimensions of 150 mm × 75 mm × 0.25 mm, the material utilized in the scheme is suitable for 6-inch 5G SP. Because the GP is on the bottom layer and the antenna feed line is on its upper surface, this board is sometimes called a Printed Circuit Board (PCB).

3.1. Antenna Design

A practical and straightforward method for lowering the MC between the distant AS is provided-the detailed strategy of a single-slot AS is displayed in Figure 1.

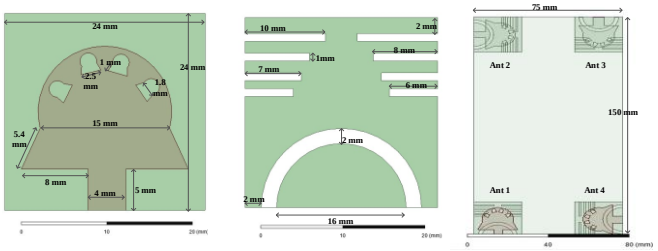

Fig. 1 (a) Strategy of proposed single element MIMO antenna with in-depth dimensions, (b) A detailed view of a slot antenna featuring open-ended, decoupled slot, and (c) Design of proposed MIMO antenna with thorough dimensions.

Eight open-ended slots with sizes ranging from 5 mm, 10 mm, 8 mm, 7 mm, and 6 mm and 1 mm in width are used. Using a rectangular feeding line at the feeding point, a semi-circular slot radiator with a size of 10 mm and a radius of 8 mm is fed into the GP. Rectangular feeding lines have been found to have the best radiation efficiency value and improved IM. For the design, HFSS was used for both modelling and simulation. Eight open-ended decoupling strips are visible on AS 1 (Ant 1).

Additionally, every other AS is positioned orthogonally to the others and shares an identical size and layout. After designing the 50-ohm feeding line, the GP's slots are created. The final slot A is tuned for optimal antenna gain and radiation efficiencies. Open-ended slot shapes reduce the mutual interaction between the antenna parts. Slots minimize MC, allowing each AS to operate independently and improving overall system effectiveness. They also aid in better IM and ensure efficient power transmission among the A and connected circuits. The slots in the GP and feedline optimize radiation efficiency, resulting in a stronger and more focused signal. If the slots in the antenna are not given, mutual coupling increases, causing interference, poor IM, reduced radiation efficiency and gain, and a larger antenna size is required.

The mutual coupling between the antennas is characterized using S parameters, which are given by

$$S_{i,j} = 10\ log_{10} \frac{P_{Received}}{P_{transmitted}}$$

$S_{i,j}$ is the isolation between ports. A lower S_{21} value indicates better isolation and minimal mutual coupling. Lower $S_{i,j}$ value means better isolation.

The mushroom-shaped antenna design was chosen for its compact structure, allowing efficient integration in limited spaces like smartphone systems. The mushroom structure enhances bandwidth and diversity performance, making it particularly suited for applications like Sub-6 GHz 5G, where both compact size and efficient radiation. With its 150 mm × 75 mm dimensions, the suggested slot antenna design is small and ideal for 5G devices with slim frames. The placement of four antennas with a distance of 75mm x 150mm aims to maximize isolation and minimize mutual coupling and electromagnetic interference between them. A large gap is provided between the antennas so that signals from each antenna do not interfere with one another. It also optimizes radiation patterns and enhances user experience with reduced hand blocking. The 75x150mm dimensions provide enough space for effective separation without wasting space within the smartphone. The 24x24mm antennas are positioned at optimal distances for compactness and performance, balancing size constraints with high isolation needs. The antennas are placed

in corner positioning in this design to achieve higher isolation, reduce interference, and ensure optimal MIMO performance for 5G SP. It also has specific benefits in performance, efficiency, and achieving the necessary MIMO functionality. Figure 2 displays the antenna structure's simulated current pattern.

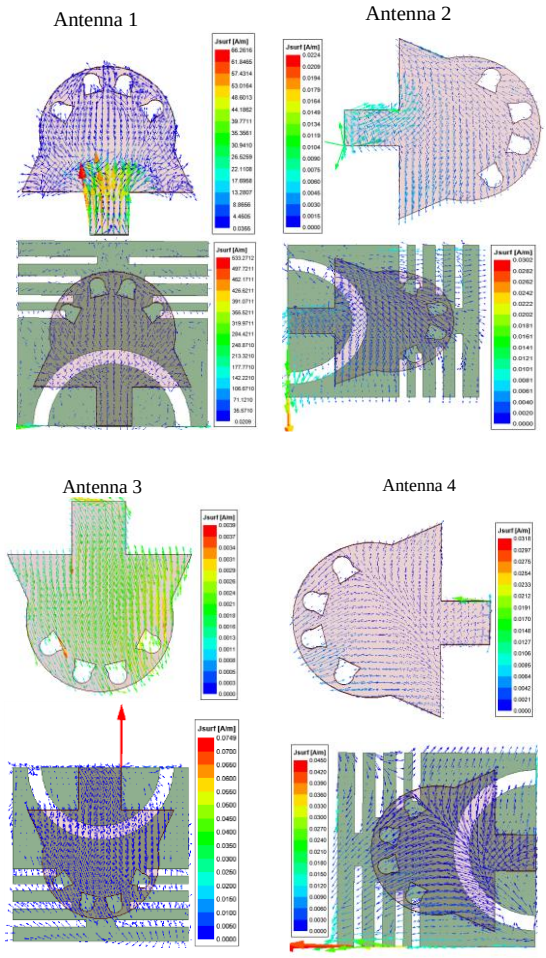

Fig. 2 Surface electric current distribution on the antenna GP at 3.4 GHz

In the case of Antenna 1 through 4, present distributions with and without DGS are shown. As observed in Figure 2, the relevant current reduces the coupling with neighbouring elements because it does not propagate in the absence of DGS surface present distribution on the suggested AS-slotted GP. As the current density increases, it is evident that a strong current flows along the slot's shorter size. In Antenna 1, the current distribution is concentrated along the larger dimensions, with the highest intensity near the feed point, as shown by the red areas. This indicates that Antenna 1 has vigorous current activity, which suggests that it can radiate efficiently, particularly along its primary axis. In Antenna 2, the current supply is more focused along the left side of the antenna, with a less intense flow overall. This implies that the antenna might radiate more directionally, dissipating less energy in unwanted directions. For Antenna 3, the current distribution is primarily oriented along the right side, as seen from the diagram. The current intensity is moderate, and the central part of the antenna experiences less current density, affecting its radiation pattern on the right side. In Antenna 4, the current is higher within the slot area than the other antennas.

This uniform current distribution throughout the antenna structure, especially in the slot region, suggests that Antenna 4 may provide better IM and more effective radiation performance. The surface current distribution predominantly concentrates around the centre of the antenna element, and the slots function as the resonator, generating the various resonant frequencies of the antenna.

The first resonance, occurring at 1.3 and 1.4 GHz, is primarily influenced by the circumference of the semicircle slot, while the second resonance, at 3.9 and 4.6 GHz, is governed by the mushroom structure. Additionally, the current along the rectangular-shaped Ms feed lines exhibits significant activity across different frequencies.

4. Results and Discussion

A comprehensive analysis of the proposed MIMO antenna system, evaluating its performance in terms of reflection coefficient, gain, VSWR, axial ratio, envelope correlation coefficient and coupling coefficient across the 1–6 GHz frequency range. A comparative assessment with existing models highlights the proposed design's superior efficiency, wider bandwidth, and improved diversity performance.

4.1. Simulation Environment

The Four-Element, Four-Port Mushroom-Shaped MIMO Antenna was simulated using ANSYS ELECTRONIC DESKTOP 2021R1-HFSS. Initially, a new HFSS project was created, and material properties were defined, selecting FR-4 as the substrate ($\varepsilon r = 4.4$, $\tan \delta = 0.02$) and copper as the conductor. The antenna structure was designed with a substrate dimension of 150 mm × 75 mm × 0.25 mm, and a Ground Plane (GP) was incorporated with semi-circular slots and eight open-ended slots to minimize mutual coupling.

Four 24 mm × 24 mm patch antennas were positioned at the corners of the substrate, each fed with a 50-ohm rectangular microstrip line. Wave ports were assigned to each feedline, creating an air box with a radiation boundary. A frequency sweep from 1 GHz to 6 GHz was performed, and S-parameters were analyzed to ensure that S21, S31, and S41 values remained below -20 dB, indicating better isolation. The 3D radiation patterns, surface current distribution, Envelope Correlation Coefficient (ECC < 0.02), gain (>5 dBi), and efficiency (>85%) were examined. The slot dimensions and feedline width were optimized for enhanced performance.

4.2. Performance Evaluation

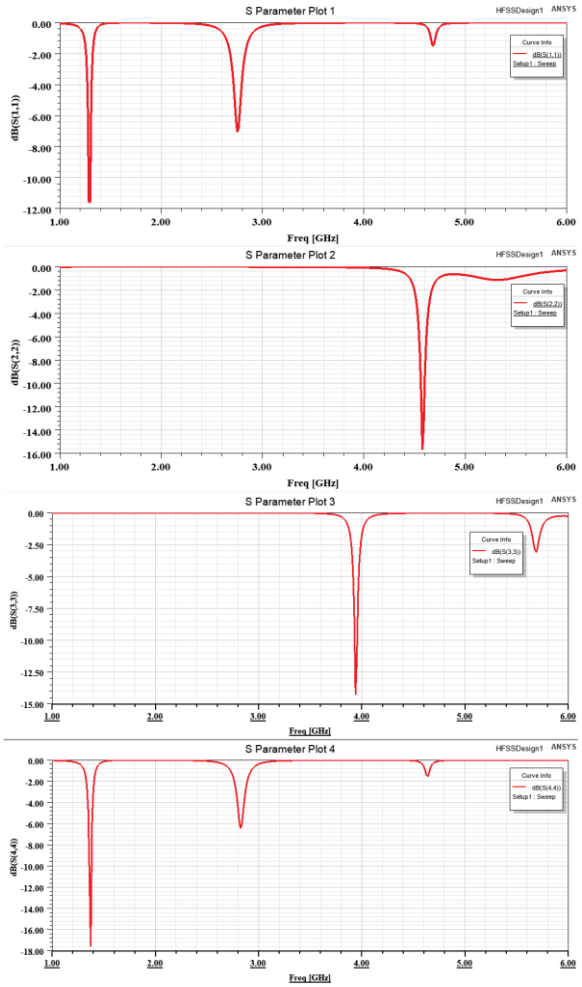

Fig. 3 Reflection coefficient for an antenna with mushroom slot

The reflection coefficient plots in Figure 3 provide the performance of four antenna ports across the FR from approximately 1 to 5 GHz. These plots show how much of the signal is reflected from each port, which indicates IM. A lower reflection coefficient (closer to -10 dB or below) indicates better matching and less signal reflection, resulting in more power transmitted through the antenna. For Port 1, the reflection coefficient shows strong resonances near 1.3 GHz, with a gain of -11.6 dB, indicating suitable impedance. Port 2 has a deep dip around 4.6 GHz, suggesting optimal matching at this frequency with an increase of -15.7 dB. Port 3 shows significant reflection suppression at around 3.9 GHz with -14.5 dB, and Port 4 demonstrates multiple resonance points at 1.4 GHz with -17.6 dB, showing effective operation at these frequencies. These plots indicate that the antennas are well-matched at different operating frequencies, with minimal signal loss due to reflection, which is essential for improving the efficacy of multi-port MIMO schemes in communication applications.

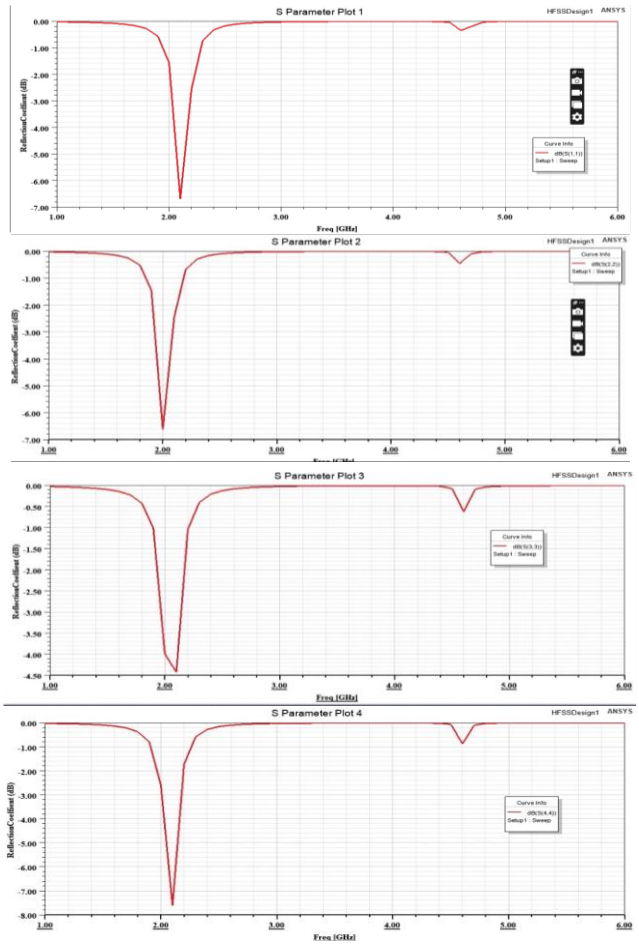

Fig. 4 Reflection coefficient for antenna without mushroom slot

The reflection factor plots in Figure 4 provide the performance of four A ports across the FR. For Port 1 to Plot 4, the reflection coefficient shows resonances near 2.05GHz, and Port 2 shows significance around 2 GHz. Port 3 shows significance at around 2.06 GHz, and Port 4 resonance points at 2.05 GHz. Table 1 shows the comparison between the reflection coefficient of the antenna with a slot and without a slot.

Table 1. Comparison between the reflection coefficient of the antenna with a slot and without a slot

Plots	Reflection coefficient with slot	Reflection coefficient without slot
Plot 1	1.3 GHz	2.05 GHz
Plot 2	4.6 GHz	2 GHz
Plot 3	3.9 GHz	2.06 GHz
Plot 4	1.4 GHz	2.3 GHz

Slots in antennas act as tuning elements, adjusting resonant frequency, IM, and radiation characteristics. They enhance IM and control electromagnetic field distribution, resulting in varied reflection coefficients in plots. The antenna with slots is a superior choice for mobile devices due to its lower reflection coefficients, multiple resonant frequencies, expanded bandwidth, and improved isolation, offering versatility and efficiency for modern communication needs in SP.

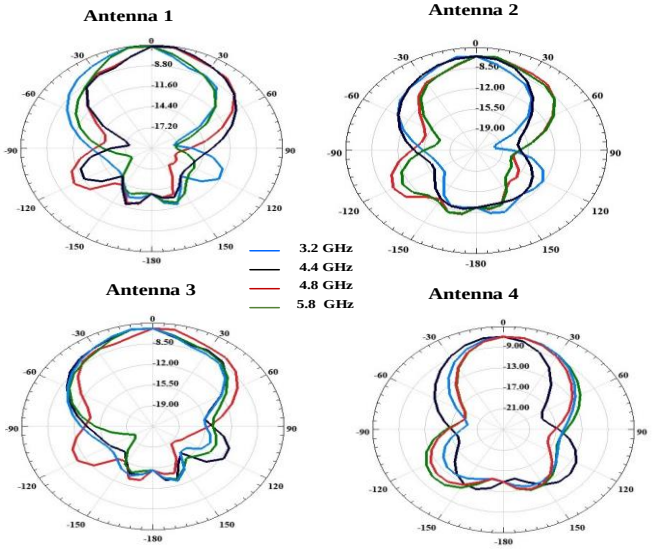

Fig. 5 Gain plots at 3.2, 4.4, 4.8 and 5.8 GHz display pattern diversity, (a) Excitation at port-1, (b) excitation at port-2, (c) excitation at port-3, and (d) excitation at port-4.

The gain plots in Figure 5 show four antennas designed for sub-6 GHz SP. Antennas 1 and 2 have narrow beams for focused signals, while Antennas 3 and 4 have wider beams for broader coverage. The image presents gain for four antennas (Antenna 1 to Antenna 4) across four FB: 3.2 GHz, 4.4 GHz, 4.8 GHz, and 5.8 GHz. The gain values (in dB) are marked on concentric circles ranging from approximately -22.5 dB to 9 dB, with each F represented by coloured lines (blue for 3.2 GHz, green for 4.4 GHz, black for 4.8 GHz, and red for 5.8 GHz). The performance of each A across these frequencies shows distinct trends.

Antenna 1 has more pronounced lobes and dips at lower frequencies (3.2 GHz and 4.4 GHz), while the gain smooths out as the F increases, reaching up to 9 dB at 5.8 GHz. Antenna 2 consistently gains across all frequencies, with the smoothest performance at 5.8 GHz. Antenna 3 exhibits more variable lobe shapes at lower frequencies but stabilizes at 4.8 GHz and 5.8 GHz, showing symmetrical gain patterns. Antenna 4 behaves similarly to Antenna 2, maintaining a uniform gain with minimal lobes and dips across all FB. Higher frequencies (4.8 GHz and 5.8 GHz) yield more stable and symmetric gain patterns across all antennas, with maximum gains around 9 dB and minimum gains around -12.5 dB. Lower frequencies (3.2 GHz and 4.4 GHz) tend to show more pronounced lobes and greater variability in gain, indicating more directional radiation. The smoother radiation patterns at higher frequencies suggest better performance for applications requiring stable gain, such as high-F communication or sensing.

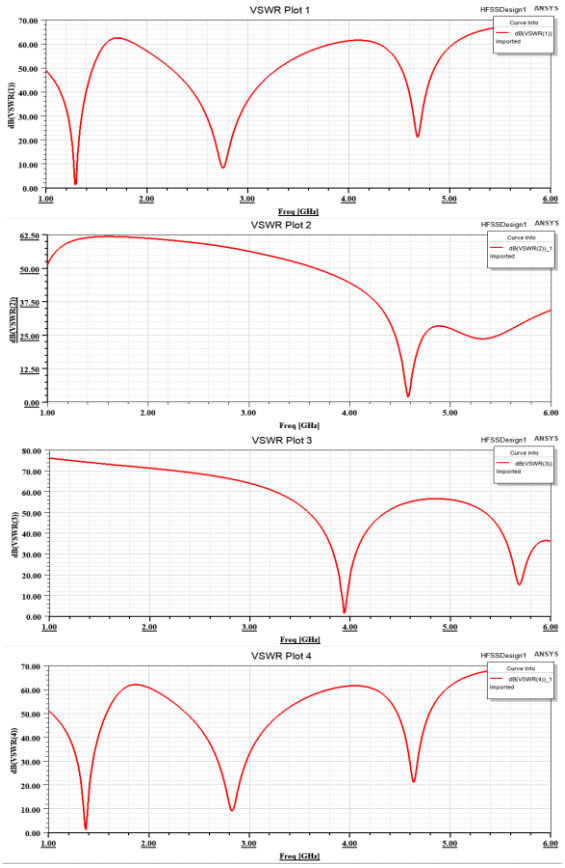

Fig. 6 VSWR Vs Frequency plots

The VSWR plots for the four antenna ports are illustrated in Figure 6, which shows the IM features over an array of frequencies. For Port 1, the antenna shows good matching around 1.5 GHz, 3.0 GHz, and 4.5 GHz, indicating efficient performance at these frequencies. Port 2 shows a broad dip near 3.5 GHz and another slight resonance at 4.58 GHz, indicating better performance in the higher FR. The plot for Port 3 demonstrates resonances at 1.6 GHz, 2.9 GHz, and 4.0 GHz, making it suitable for mid-range frequencies. Similarly, Port 4 shows resonance dips at 1.39 GHz, 2.8 GHz, and 4.5 GHz, making it effective across multiple bands. Overall, Ports 1 and 4 exhibit broader multi-band matching, while Ports 2 and 3 show better performance around 4 GHz. Low VSWR values at resonances indicate efficient operation at corresponding frequencies, which is crucial for minimizing signal reflection and maximizing power transmission. Table 2 illustrates the VSWR vs frequency plot for the proposed model.

Table 2. VSWR vs Frequency for the proposed model

No of ports	Frequency (GHz)	VSWR (dB)
Port 1	1.50	1.5
Port 2	4.58	1.8
Port 3	4.00	1.75
Port 4	1.39	1.6

4.3. Comparative Study

The Axial Ratio (AR) is a key parameter for assessing the performance of Circularly Polarised (CP) antennas. The first step is to measure the AR to determine if a CP antenna meets system requirements. This is typically done by receiving the transmitted signal from the CP antenna with a linearly polarised AS, which is revolved at different axial angles. The outcome of the ellipse's major-to-minor axis ratio is known as the AR.

The purpose of a CP antenna is to produce two orthogonal electric field portions with a 90° phase deviation and equal intensities. Once the signal radiates from the antenna aperture, it produces a circularly or elliptically polarised wave in free space.

The graph shows in Figure 7 the Axial Ratio (AR) in dB versus Frequency (GHz) for different antenna lengths (L = 17 mm, 18 mm, 19 mm, 20 mm, and 21 mm) in the 1–6 GHz range. For effective Circular Polarization (CP), the axial ratio should be ≤ 3 dB. The L = 17 mm and L = 18 mm cases exhibit high AR values (> 5 dB) over most frequency ranges, indicating poor circular polarization and more linear behavior.

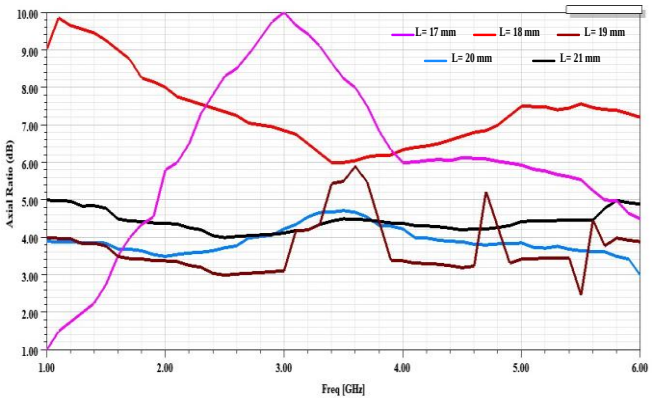

Fig. 7 Axial ratio

The L = 19 mm case shows improved performance, maintaining AR around 3 dB in certain bands but still exceeding this threshold at various points. The L = 20 mm and L = 21 mm cases demonstrate the best CP performance, with AR values staying closer to 3 dB or lower across a wider bandwidth, particularly around 2.5–5.5 GHz. This suggests that L = 20 mm and L = 21 mm provide better axial ratio performance for circular polarization, as shown in Table 3, within the desired frequency range.

Table 3. Axial ratio values of the proposed model

Frequency	L=17 (pink)	L=18 (Red)	L=19 (Brown)	L=20 (Blue)	L=21 (Black)
1	0.9	8.9	3.9	3.8	4.8
2	5.7	7.9	3.3	3.4	4.2
3	9.8	6.8	3.0	4.2	4.04
4	5.9	6.3	3.3	4.24	4.36
5	5.9	7.4	3.3	3.8	4.4
6	4.4	7.1	3.8	2.9	4.9

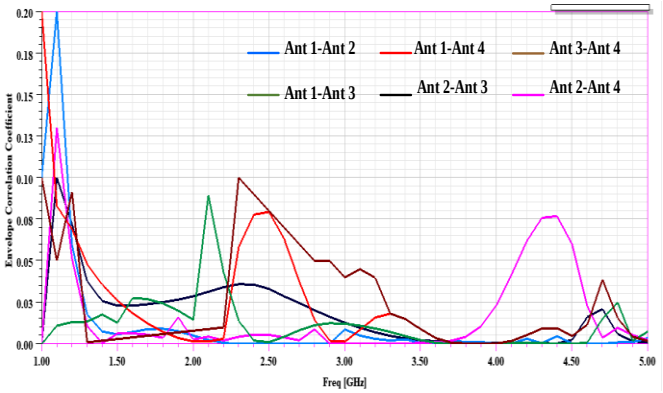

Fig. 8 Envelope Correlation Coefficient (ECC)

To assess the MIMO efficiency of the suggested AS, it is essential to analyze the ECC parameters. ECC can be derived from the complex S parameters of each individual AS employing the following equations:

$$ECC = \frac{\left|Z_{ii}^{*}Z_{ij} + Z_{ij}^{*}Z_{jj}\right|}{\left(1 - |Z_{ii}|^{2} - \left|Z_{ij}\right|^{2}\right) - \left(1 - \left|Z_{ij}\right|^{2} - \left|Z_{jj}\right|^{2}\right)^{*}}$$

Figure 8 depicts the ECC results remain consistently low, below 0.2, across the entire bandwidth. Furthermore, the ECC is smaller than 0.04 throughout the FR. These findings indicate that the adjacent elements have minimal correlation with each other.

This plot shows in Figure 8 the Envelope Correlation Coefficient (ECC) for six different MIMO antenna pairings (Ant1–2, Ant1–3, Ant1–4, Ant2–3, Ant2–4, and Ant3–4) across the 1–5 GHz band. Overall, ECC values stay well

below 0.2 for most frequencies, which is good for MIMO performance (the usual target is ECC < 0.5 and ideally < 0.1). Around 1.0 GHz, Ant1–Ant2 briefly peaks at about 0.20, then drops below 0.05 for the rest of the band. Ant3–Ant4 remains below 0.1 through much of the mid-band but rises to about 0.18 near 4.5–5.0 GHz. The other antenna pairs (Ant1–4, Ant3–4, Ant2–3, Ant1–3) generally stay between 0.00 and 0.08 throughout the 1–5 GHz range. These low ECC values indicate good isolation and diversity performance among the antenna elements, which is favorable for MIMO applications. Table 4 shows the ECC values for various antennae of the proposed model.

Table 4. ECC value for the proposed model

Frequency (GHz)	Ant 1-2 (blue)	Ant 1-3 (Green)	Ant 1-4 (Red)	Ant 2-3 (Brown)	Ant 2-4 (Black)	Ant 3-4 (Pink)
1	0.106	0.005	0.198	0.005	0.005	0.099
2	0.006	0.028	0.002	0.035	0.027	0.007
3	0.009	0.012	0.008	0.015	0.012	0.039
4	0.002	0.007	0.001	0.001	0.014	0.023
5	0.004	0.004	0.001	0.002	0.001	0.001

Table 5. Coupling coefficient value of the proposed model

Frequency (GHz)	S (1-2) (dB)	S (1-4) (dB)	S (2-4) (dB)	S (1-3) (dB)	S (2-3) (dB)	S (3-4) (dB)
1	-65.8	-77.2	-86.25	-85.48	-75.73	-87.50
2	-68.9	-83.3	-100.31	-79.01	-75.93	-88.76
3	-75.9	-83.07	-116.1	-88.20	-86.92	-87.69
4	-89.8	-82.76	-112.7	-98.67	-86.86	-79.68
5	-89.5	-75.27	-109.3	-89.63	-97.33	-66.28
6	-75.3	-81.37	-78	-74.70	-91.38	-55.20

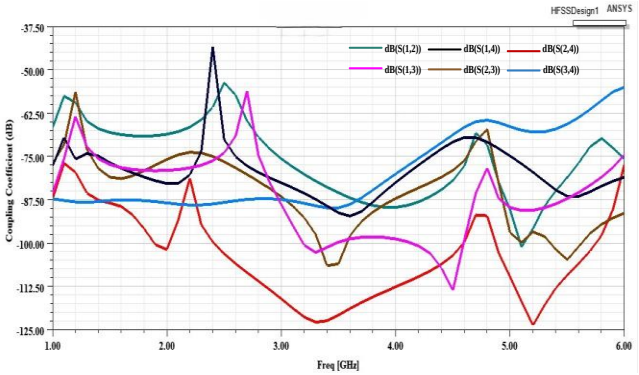

Fig. 9 Coupling coefficient

The outcomes of the modeling are shown in Figure. 9, which also examines the impact of MC among the four ports. Among the MIMO antenna ports, a comparatively high decoupling was attained, with mutual coupling values kept almost below -55 dB across the majority of the operating bandwidth. The design achieves an exceptional decoupling level of -122 dB at 5.2 GHz, demonstrating the effectiveness of the DGS and the mushroom-shaped features in reducing interference among the AS.

This low mutual coupling is critical for enhancing the overall performance, ensuring minimal cross-talk and allowing each antenna element to function independently, thereby improving signal quality, increasing channel capacity, and reducing transmission errors. The significant isolation across the sub-6 GHz FR makes this antenna system well-suited for high-performance 5G applications, ensuring reliable, efficient, and interference-free communication even in dense multipath environments. The coupling coefficient values are given in Table 5.

4.3.1. Comparison Metric with Conventional Methods

Comparative analysis of various proposed MIMO antennas shown in Table 6 (150 × 75 × 0.25 mm) outperforms existing designs by offering a broader frequency range (1–6 GHz), higher isolation (-20 dB), superior gain (9–12.5 dB), and lower ECC (<0.02), making it ideal for modern wireless applications.

Unlike previous models that operate at limited frequency bands such as 2.5 GHz, 4.72–5.24 GHz, and 28 GHz, the proposed design provides continuous spectrum coverage, ensuring greater versatility. It also achieves a higher gain compared to prior designs like [26] (1.74 dB) and [25] (2.73 dB) while maintaining better isolation (-20 dB), surpassing designs with unreported isolation values.

Additionally, the low ECC (<0.02) enhances diversity performance, reducing interference and improving overall signal quality. With these advancements, the proposed model presents a compact, high-performance solution for Sub-6 GHz 5G applications, ensuring improved efficiency and reliability over existing MIMO antenna designs.

Table 6. Comparative analysis of various proposed models

Reference Number	Shape of Antennas	Dimension (mm)	Number of Antennas	Frequency (GHz)	Isolation (dB)	Gain (dB)	ECC
[24]	Four Element E and C-shaped slot	46x46x1.6	4	4.72-5.24	-	2.73	<0.006
[25]	Quadrilateral patch antenna with four rectangular holes	17.76x17.76x1.52	4	28	-39	9	$3.6x10^{-5}$
[26]	Lower rectangular-shaped patch with a pair of ellipses on its edges	70x70x1.6	4	2.5	>28	1.74	<0.5
Proposed Model	Four-Element Four-Port Mushroom-shaped	150x75x0.25	4	1-6	-20	12.5-9	<0.02

5. Future Research Direction

Future research will focus on extending the antenna design to higher frequency bands, such as the millimetre-wave spectrum, while maintaining efficiency and compactness for next-generation wireless communication. This includes designing the topology to support sub-6 GHz and mm-Wave 5G bands, ensuring seamless integration into future smartphone models. Additionally, to achieve further miniaturization, improved gain, and enhanced overall performance, research will explore new substrate materials with higher permittivity and lower loss. Real-world testing or case studies demonstrating the application of the antenna prototype in actual smartphone devices will be crucial in assessing performance under various conditions, such as interference, multipath fading, and user interaction effects. Field trials in actual 5G and emerging 6G networks will help evaluate reliability, signal integrity, and robustness in real-world deployments. These advancements will enhance bandwidth, data rates, and spatial multiplexing capabilities and ensure that the antennas meet the evolving demands of future wireless technologies.

6. Conclusion

The four-element, four-port, mushroom-shaped MIMO antenna system presented in this research is intended for 5G smartphone applications operating at frequencies lower than 6 GHz. The system incorporates mushroom resonators and Defected Ground Structures, improving isolation and polarization diversity. Mutual coupling is reduced to below -15 dB across all elements. The reflection coefficient remains below -10 dB for most frequencies, and the Envelope Correlation Coefficient (ECC) remained under 0.04 throughout the 1-5 GHz range, ensuring excellent MIMO performance.

The antenna provides strong radiation patterns and bandwidth coverage, particularly at key frequencies like 1.3 GHz, 3.9 GHz, and 4.6 GHz, making it suitable for next-generation 5G smartphones. The optimized MIMO configuration enhances signal reliability, reduces interference, and increases spectral efficiency, making it ideal for urban and indoor deployments. The compact design ensures seamless integration into a slim smartphone chassis, maintaining device aesthetics while maximizing radiation efficiency.

Additionally, the reduction in mutual coupling enhances multi-antenna performance, supporting better beamforming and spatial multiplexing, which are crucial for high-speed data transmission in 5G networks. Future work will focus on extending the design to cover higher frequency bands and exploring new materials exploration for improved effectiveness in 5G and emerging 6G applications.

References

[1] Zhe Chen et al., "An Ultra-Wideband MIMO Antenna for 5G Smartphone," *AEU - International Journal of Electronics and Communications*, vol. 154, 2022. [CrossRef] [Google Scholar] [Publisher Link]

[2] Arun Raj et al., "Design and Analysis of Square Shape Slot Cut High Gain Sierpinski Carpet Fractal Antenna for Wireless Applications," *Microwave and Optical Technology Letters*, vol. 65, no. 8, pp. 2337-2343, 2023. [CrossRef] [Google Scholar] [Publisher Link]

[3] Xi Wang, and Yuandan Dong, "A Four-Port MIMO Antenna System for 5G Mobile Terminals," *IEEE Asia-Pacific Microwave Conference*, Hong Kong, pp. 69-71, 2020. [CrossRef] [Google Scholar] [Publisher Link]

[4] Thennarasi Govindan et al., "Conformal Quad-Port UWB MIMO Antenna for Body-Worn Applications," *International Journal of Antennas and Propagation*, vol. 2021, no. 1, pp. 1-13, 2021. [CrossRef] [Google Scholar] [Publisher Link]

[5] Jayshri Kulkarni et al., "Design and Analysis of Wideband Flexible Self-Isolating MIMO Antennas for Sub-6 GHz 5G and WLAN Smartphone Terminals," *Electronics*, vol. 10, no. 23, pp. 1-21, 2021. [CrossRef] [Google Scholar] [Publisher Link]

[6] Muhannad Muhsin et al., "The Multi Input Multi Output Antenna Array Design for 5G N78 Applications in Smartphones," *Al-Rafidain Journal of Engineering Sciences*, vol. 1, no. 1, 2023. [CrossRef] [Google Scholar] [Publisher Link]

[7] Hirald Dwaraka Praveena et al., "A Compact Square and Hexagonal Antennas with Fractal DGS for Mobile Satellite Applications," *Journal of Pharmaceutical Negative Results*, vol. 13, no. 4, pp. 962-967, 2022. [CrossRef] [Google Scholar] [Publisher Link]

[8] Vipul Kaushal, Amit Birwal, and Kamlesh Patel, "Diversity Characteristics of Four-Element Ring Slot-Based MIMO Antenna for Sub-6-GHz Applications," *ETRI Journal*, vol. 45, no. 4, pp. 581-593, 2023. [CrossRef] [Google Scholar] [Publisher Link]

[9] Muhammad Noaman Zahid et al., "H-Shaped Eight-Element Dual-Band MIMO Antenna for Sub-6 GHz 5G Smartphone Applications," *IEEE Access*, vol. 10, pp. 85619-85629, 2022. [CrossRef] [Google Scholar] [Publisher Link]

[10] Niamat Hussain, and Nam Kim, "Integrated Microwave and mm-Wave MIMO Antenna Module with 360° Pattern Diversity for 5G Internet of Things," *IEEE Internet of Things Journal*, vol. 9, no. 24, pp. 24777-24789, 2022. [CrossRef] [Google Scholar] [Publisher Link]

[11] Ubaid Ullah et al., "Implementation of Spatial/Polarization Diversity for Improved-Performance Circularly Polarized Multiple-Input-Multiple-Output Ultra-Wideband Antenna," *IEEE Access*, vol. 8, no. 64112-64119, 2020. [CrossRef] [Google Scholar] [Publisher Link]

[12] Sabah Hassan Ghadeer et al., "An Innovative Fractal Monopole MIMO Antenna for Modern 5G Applications," *AEU - International Journal of Electronics and Communications*, vol. 159, pp. 1-16, 2023. [CrossRef] [Google Scholar] [Publisher Link]

[13] Naveen Jaglan, Samir Dev Gupta, and Mohammad S. Sharawi, "18 Element Massive MIMO/Diversity 5G Smartphones Antenna Design for Sub-6 GHz LTE Bands 42/43 Applications," *IEEE Open Journal of Antennas and Propagation*, vol. 2, pp. 533-545, 2021. [CrossRef] [Google Scholar] [Publisher Link]

[14] Munusami Cholavendan, and Venkatesan Rajeshkumar, "Dual-Feed Orthogonally Polarized Compact 8-Element MIMO Antenna Using Metallic Stub and Decoupling Unit for Isolation Enhancement of Sub-6 GHz 5G Application," *Progress in Electromagnetics Research Letters*, vol. 116, pp. 105-111, 2024. [CrossRef] [Google Scholar] [Publisher Link]

[15] D. El Hadri et al., "Dual-Band MIMO Antenna with Four CPW Elements Using Polarization Diversity for 5G Mobile Communication Networks and Satellite," *Advanced Electromagnetics*, vol. 12, no. 3, pp. 43-53, 2023. [Google Scholar] [Publisher Link]

[16] Saad Hassan Kiani et al., "Dual-Polarized Wideband 5G N77 Band Slotted MIMO Antenna System for Next-Generation Smartphones," *IEEE Access*, vol. 12, pp. 34467-34476, 2024. [CrossRef] [Google Scholar] [Publisher Link]

[17] Naser Ojaroudi Parchin et al., "Four-Element/Eight-Port MIMO Antenna System with Diversity and Desirable Radiation for Sub 6 GHz Modern 5G Smartphones," *IEEE Access*, vol. 10, pp. 133037-133051, 2022. [CrossRef] [Google Scholar] [Publisher Link]

[18] Nada M. Khalil Al-Ani et al., "A Dual-Polarized MIMO Array Antenna System for Future Smartphone," *Journal of Physics: Conference Series, IOP Publishing, International Conference of Modern Applications on Information and Communication Technology*, Babylon-Hilla City, Iraq, vol. 1804, no. 1, pp. 1-9, 2021. [CrossRef] [Google Scholar] [Publisher Link]

[19] Prutha Kulkarni, and Raju Srinivasan, "Compact Polarization Diversity Patch Antenna in L and WiMAX Bands for IoT Applications," *AEU - International Journal of Electronics and Communications*, vol. 136, 2021. [CrossRef] [Google Scholar] [Publisher Link]

[20] Mohammad M. Fakharian, "A Massive MIMO Frame Antenna with Frequency Agility and Polarization Diversity for LTE and 5G Applications," *International Journal of RF and Microwave Computer-Aided Engineering*, vol. 31, no. 10, 2021. [CrossRef] [Google Scholar] [Publisher Link]

[21] Nizar Sghaier, and Lassaad Latrach, "Design and Analysis of Wideband MIMO Antenna Arrays for 5G Smartphone Application," *International Journal of Microwave and Wireless Technologies*, vol. 14, no. 4, pp. 511-523, 2022. [CrossRef] [Google Scholar] [Publisher Link]

[22] Nada Alaa et al., "Q-Band MIMO Antennas with Circular Polarization for Spatial and Polarization Diversity," *Journal of Infrared, Millimeter, and Terahertz Waves*, vol. 45, pp. 393-432, 2024. [CrossRef] [Google Scholar] [Publisher Link]

[23] Prashant Chaudhary, Ashwani Kumar, and B.K. Kanaujia, "A Low-Profile Wideband Circularly Polarized MIMO Antenna with Pattern and Polarization Diversity," *International Journal of Microwave and Wireless Technologies*, vol. 12, no. 4, pp. 316-322, 2023. [CrossRef] [Google Scholar] [Publisher Link]

[24] Sachin S. Khade et al., "Four Element EC Slot MIMO Antenna for WLAN, Wi-Fi and 5G Applications," *Progress in Electromagnetics Research C*, vol. 139, pp. 147-158, 2023. [CrossRef] [Google Scholar] [Publisher Link]

[25] Rania Hamdy Elabd, and Ahmed Jamal Abdullah Al-Gburi, "Ultra-Compact 4-Port MIMO Antenna with Defected Ground Structure and SAR Analysis for 28/38 GHz 5G Mobile Devices," *Journal of Electromagnetic Waves and Applications*, vol. 38, no. 9, pp. 1000-1025, 2024. [CrossRef] [Google Scholar] [Publisher Link]

[26] Ghanshyam Singh et al., "Frequency Reconfigurable Quad-Element MIMO Antenna with Improved Isolation for 5G Systems," *Electronics*, vol. 12, no. 4, pp. 1-17, 2023. [CrossRef] [Google Scholar] [Publisher Link]